

Article

A Synergy Approach to Enhance Upconversion Luminescence Emission of Rare Earth Nanophosphors with Million-Fold Enhancement Factor

Duc Tu Vu ^{1,2}, Yi-Chang Tsai ¹, Quoc Minh Le ³, Shiao-Wei Kuo ⁴, Ngoc Diep Lai ⁵, Henri Benisty ⁶, Jiunn-Yuan Lin ^{1,7}, Hung-Chih Kan ^{1,7} and Chia-Chen Hsu ^{1,7,*}

- ¹ Department of Physics, National Chung Cheng University, Ming Hsiung, Chiayi 621, Taiwan; tu.vuduc@phenikaa-uni.edu.vn (D.T.V.); hp2avatar1170@hotmail.com.tw (Y.-C.T.); phyjyl@ccu.edu.tw (J.-Y.L.); phyhck@ccu.edu.tw (H.-C.K.)
- ² Faculty of Electrical and Electronics Engineering, Phenikaa University, Yen Nghia, Ha Dong, Hanoi 12116, Vietnam
- ³ Institute of Materials Science, Graduate University of Science and Technology, Vietnamese Academy of Science and Technology (VAST), 18 Hoang Quoc Viet, Cau Giay, Hanoi 100.000, Vietnam; lequocminhvn@gmail.com
- ⁴ Department of Materials and Optoelectronic Science, National Sun Yat-sen University, Kaohsiung 804, Taiwan; kuosw@faculty.nsysu.edu.tw
- ⁵ Laboratoire Lumière, Matière et Interfaces (LuMin), Institut D'Alembert, CNRS, Ecole Normale Supérieure Paris-Saclay, Université Paris-Saclay, CentraleSupélec, 4 Avenue des Sciences, 91190 Gif-sur-Yvette, France; ngoc-diep.lai@ens-paris-saclay.fr
- ⁶ Laboratoire Charles Fabry, CNRS, Institut d'Optique Graduate School, Université Paris-Saclay, 91127 Palaiseau, France; henri.benisty@institutoptique.fr
- ⁷ Center for Nano Bio-Detection, National Chung Cheng University, Ming Hsiung, Chiayi 621, Taiwan
- * Correspondence: phycch@ccu.edu.tw



Citation: Vu, D.T.; Tsai, Y.-C.; Le, Q.M.; Kuo, S.-W.; Lai, N.D.; Benisty, H.; Lin, J.-Y.; Kan, H.-C.; Hsu, C.-C. A Synergy Approach to Enhance Upconversion Luminescence Emission of Rare Earth Nanophosphors with Million-Fold Enhancement Factor. *Crystals* **2021**, *11*, 1187. <https://doi.org/10.3390/cryst11101187>

Academic Editor: Marilena Carbone

Received: 25 August 2021

Accepted: 24 September 2021

Published: 29 September 2021

Publisher's Note: MDPI stays neutral with regard to jurisdictional claims in published maps and institutional affiliations.



Copyright: © 2021 by the authors. Licensee MDPI, Basel, Switzerland. This article is an open access article distributed under the terms and conditions of the Creative Commons Attribution (CC BY) license (<https://creativecommons.org/licenses/by/4.0/>).

Abstract: Lanthanide (Ln^{3+})–doped upconversion nanoparticles (UCNPs) offer an enormous future for a broad range of biological applications over the conventional downconversion fluorescent probes such as organic dyes or quantum dots. Unfortunately, the efficiency of the anti–Stokes upconversion luminescence (UCL) process is typically much weaker than that of the Stokes downconversion emission. Albeit recent development in the synthesis of UCNPs, it is still a major challenge to produce a high–efficiency UCL, meeting the urgent need for practical applications of enhanced markers in biology. The poor quantum yield efficiency of UCL of UCNPs is mainly due to the following reasons: (i) the low absorption coefficient of Ln^{3+} dopants, the specific Ln^{3+} used here being ytterbium (Yb^{3+}), (ii) UCL quenching by high–energy oscillators due to surface defects, impurities, ligands, and solvent molecules, and (iii) the insufficient local excitation intensity in broad-field illumination to generate a highly efficient UCL. In order to tackle the problem of low absorption cross-section of Ln^{3+} ions, we first incorporate a new type of neodymium (Nd^{3+}) sensitizer into UCNPs to promote their absorption cross-section at 793 nm. To minimize the UCL quenching induced by surface defects and surface ligands, the Nd^{3+} -sensitized UCNPs are then coated with an inactive shell of NaYF_4 . Finally, the excitation light intensity in the vicinity of UCNPs can be greatly enhanced using a waveguide grating structure thanks to the guided mode resonance. Through the synergy of these three approaches, we show that the UCL intensity of UCNPs can be boosted by a million–fold compared with conventional Yb^{3+} –doped UCNPs.

Keywords: upconversion nanoparticles; upconversion luminescence; Nd^{3+} sensitizer; surface passivation; guided mode resonance; resonant waveguide grating

1. Introduction

Upconversion luminescence (UCL) of lanthanide (Ln^{3+})–doped upconversion nanoparticles (UCNPs) is a nonlinear optical process involving the sequential absorption of near-

infrared (NIR) photons and/or energy transfer (ET) processes, followed by the emission of high-energy photons in ultraviolet (UV), visible (VIS), or NIR regions [1–6]. UCNP have attracted enormous interest in the past few years because of their exceptional physicochemical properties such as narrow emission bandwidths, superior photostability, low background signal, long luminescence lifetime (\approx ms), no blinking, as well as no photobleaching [7–9]. Furthermore, UCL emission can be generated with NIR excitation sources within the first biological window range of 750–950 nm, favoring their use as bioprobes for bioimaging applications. The excitation light with a wavelength inside the first biological window range permits a relatively large penetration depth in biotissues, low autofluorescence background, and minimal absorption of biomolecules, thus providing a high-contrast deep-tissue luminescence bioimage compared to the use of the conventional downshifting fluoroprobes [10–12].

For real usage in biological fields, an ideal fluoroprobe should generally meet several criteria, such as intense emission, monodispersity, small size, biocompatibility, and non-toxicity [13]. Recently, Ln^{3+} -doped UCNP are emerging as a booming material for biological applications [10–16]. Particularly with the development of facile and versatile strategies for surface modification [17], biocompatible and low biotoxicity UCNP have opened a variety of applications in biomedical fields such as imaging [16,18,19], fluorescence assays [20], biosensing [21], molecular detection [22], drug delivery [23], and therapeutics [16,24]. Nevertheless, the UCL intensity of UCNP is still incomparable with their bulk counterparts and single-photon excited nanomaterials, i.e., organic dyes or quantum dots [12,23,24]. In fact, one typical type of UCNPs, i.e., ytterbium (Yb^{3+})-doped UCNP, frequently suffer from extremely low quantum yields (typically $< 1\%$) owing to the relatively low absorption coefficient of Yb^{3+} dopants [25,26]. The large surface-to-volume ratio in nanometer-size UCNP results in non-radiative decay induced by the surface defects, diminishing UCL efficiency. Additionally, the existence of surface ligands or solvent molecules with high-energy vibrational modes, e.g., O–H, C–H, or N–H groups, matching with phonon modes of the host material can lead to non-radiative multiphonon relaxation. As is well-known, oleic acid, a common surfactant used in the synthetic process of UCNP, possesses high vibrational energies and thus causes non-radiative energy losses in the UCL process. Another adverse factor for biocompatible UCNP is the attainment of high water solubility. As hydrophilic UCNP are dispersed into an aqueous environment for biomedical applications, the quenching effect induced by aqueous solution is even stronger compared to organic solutions, arising from the high-energy vibrations of hydroxyl groups [17]. Therefore, the utilization of UCNP as fluoroprobe often needs a rather high excitation intensity and/or high concentration of nanoparticles, which may induce several detrimental side effects during diagnosis or treatment, such as overheating or poisoning issues. From this point of view, the Ln^{3+} -doped UCNP and particularly Yb^{3+} -doped UCNP are still not ready for biomedical applications and commercialization, thereby implying that it is particularly important and urgent to further improve the UCL efficiency of UCNP.

Hence, one of the major driving forces and the main challenges for research in the realm of UCNP technology is the improvement of UCL efficiency of UCNP, as depicted above. Strategies to enhance the UCL efficiency of UCNP can be classified into two broad categories: (a) nanoparticles engineering and (b) photonic engineering [27–29]. The techniques used for nanoparticles engineering typically involve host lattice manipulation, energy transfer modulation, surface passivation, and neodymium (Nd^{3+}) sensitization. On the other hand, photonic engineering comprises two main approaches: plasmonic nanostructures and dielectric nanostructures [27–29].

In nanoparticle engineering, the absorption strength and emission rate of UCNP can be tuned by varying the ingredients and synthesis conditions of UCNP. Surface passivation, by coating a uniform shell around a core, is considered as a key approach to enhance UCL efficiency. In such core@shell (CS) structures, dopant Ln^{3+} ions are spatially distributed in the inner core of UCNP to minimize and ideally block non-radiative ET

from luminescent dopants to surface defects. This approach is particularly effective for nanometer-size UCNPs because of their high surface-to-volume ratio. A great deal of strategies have been developed for the synthesis of high-quality CS UCNPs, which can be categorized into three major types: amorphous, inactive, and active shells [30–32]. Recently, Nd³⁺ sensitization, with additional doping of Nd³⁺ ions in the shell layer of Yb³⁺-doped UC nanocrystals, appeared as an efficacious way to improve the UCL efficiency of UCNPs [19,33–39]. As is well known, the excitation wavelength can be tuned from 980 to 793 nm in the Nd³⁺-Yb³⁺ co-doped UC system, thanks to a combination of Nd³⁺ and Yb³⁺ in which Nd³⁺ serves as a sensitizer and Yb³⁺ acts as an energy mediator. Advantages for Nd³⁺ doping of the traditional Yb³⁺-sensitized UCNPs include (i) the use of a 793 nm NIR laser as the excitation source can settle the low penetration depth of tissue, as well as overheating issues of using the 980 nm excitation light [34–36], (ii) the absorption cross-section of Nd³⁺ ($1.2 \times 10^{-19} \text{ cm}^2$ at 793 nm) is one order of magnitude higher than that of Yb³⁺ ($1.2 \times 10^{-20} \text{ cm}^2$ at 980 nm) [19], (iii) the Nd³⁺-Yb³⁺ ET efficiency can be as high as 70%, depending on the percentage of Nd³⁺ ion experiencing ET among all excited Nd³⁺ ions, which thus facilitates the brightness of UCL emission [19]. The Nd³⁺ ions are often selectively doped in the shell layer to avoid the quenching of UCL emission caused by energy back transfer from activators (erbium (Er³⁺), thulium (Tm³⁺), and holmium (Ho³⁺)) to ⁴I_j manifolds of Nd³⁺ [39]. It is worth noting that a suitable concentration of Yb³⁺ also needs to be co-doped with Nd³⁺ in the shell layer to facilitate successive Nd³⁺ → Yb³⁺ → activator (Tm³⁺) ET processes. However, the surface luminescence quenching effect induced by Nd³⁺ and Yb³⁺ dopants in the shell layer is another significant constraint. Consequently, the more complex core@shell@shell (CSS) multilayer UCNPs were developed by adding a coating of an inactive shell layer (NaYF₄) on the CS structure to passivate the surface defects [36].

The main concept of photonic engineering is to use plasmonic nanostructures or dielectric nanostructures to create a strong local field near UCNPs at their absorption wavelength, which enhances the absorption rate of UCNPs through the excitation resonance effect and thus dramatically increases the UCL intensity of UCNPs. For example, if a plasmonic nanostructure or dielectric nanostructure can increase the local field intensity about 10^{*m*}-fold, this will promote the UCL intensity of UCNPs by 10^{*m*} times with *n* > 1. That is because the UCL process is a multiphoton process and it follows $I_{UCL} = I_{exc}^n$, where I_{UCL} , I_{exc} , and *n* are UCL intensity, excitation intensity, and the (effective) number of absorbed photons involved in the UCL process, respectively [28]. The other way in the photonic engineering category to improve the UCL efficiency of UCNPs is to use plasmonic nanostructures or dielectric nanostructures to increase the local photon density of states at the emission wavelength of UCNPs. This is the case of the so-called extraction resonance effect, in which the resonance wavelength of the nanostructures is tuned to match with the emission wavelength of UCNPs. The extraction resonance effect can increase the radiative decay rate of UCL through the Purcell effect [40]. However, the enhancement factor provided by the extraction resonance effect is typically much less than that offered by the excitation resonance effect, which is mostly because very strong Purcell effects (from photonic crystals, metal-insulator-metal sandwiches structures, etc.) arise only at a few scarce “hot spots” of minute volume where biological molecules have to be attracted by some means, whereas the directional excitation light already funneled in few optical modes (one ideally) can be enhanced in plane or surface geometries that are truly extended. Although the local field enhancement provided by dielectric nanostructures is typically smaller than that of plasmonic nanostructures, dielectric nanostructures do not suffer parasitic energy losses manifested by fluorescence quench caused by the metal’s electron gas through its many internal degrees of freedom (Joule losses). Through proper design of the structure, some dielectric nanostructures can enhance the UCL of UCNPs more than 100 times [28,41–47]. A variety of dielectric nanostructures, such as photonic crystals [28,41–44], and metasurfaces [45–47] have been employed to enhance the UCL of UCNPs. Recently, we demonstrated that the UCL of UCNPs can be enhanced more

than 1000-fold by depositing UCNPs atop a resonant waveguide grating (RWG) structure, also termed 1D photonic crystal substrate, thanks to its guided mode resonance (GMR) to promote the local field of the excitation light atop the RWG [41,42].

In this work, we combined both nanoparticles and photonic engineering approaches to tackle the low UCL efficiency problem of Yb^{3+} -doped UCNPs. In the nanoparticle engineering aspect, Nd^{3+} ions were incorporated into the UCNP lattice to serve as sensitizers to promote the excitation light absorption of UCNPs at 793 nm wavelength. Furthermore, the outer surface of UCNPs was coated with an inactive shell of NaYF_4 to reduce UCL quench from surface defects and surface-associated ligands (see Figure 1a,b). For the photonic engineering, a low refractive index (low- n) RWG structure (Figure 1c), which offers a favorable guided mode profile, was employed to enhance the absorption rate of UCNPs through the *excitation resonance effect* and the radiative decay rate of UCL via the *extraction resonance effect*, thanks to the GMR effect offered by the low- n RWG structure. Combining these three approaches, the UCL intensity of UCNPs was eventually enhanced over a million-fold compared with conventional Yb^{3+} -doped UCNPs.

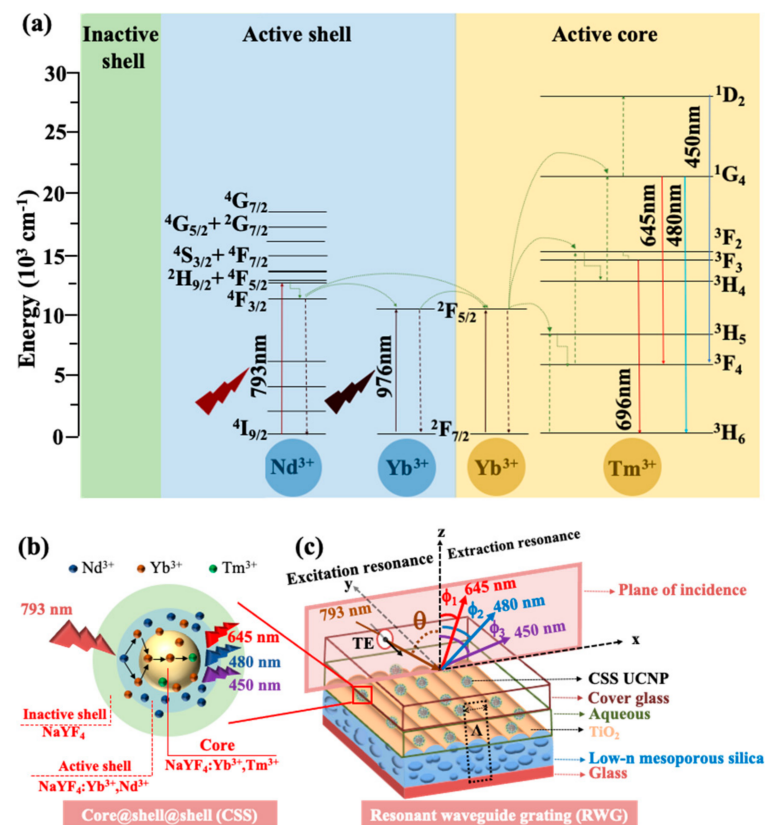


Figure 1. (a) Illustration of the proposed energy-level diagram describing the proposed UCL processes for Nd^{3+} , Yb^{3+} , and Tm^{3+} ions. The full, zigzag, curved, and dashed arrows denote excitation, multiphonon relaxation, energy transfer, and emission processes, respectively. (b) Design of the core@shell@shell UCNPs. (c) Schematic of the UCNPs-deposited low- n RWG structure, in which the core@shell@shell UCNPs were deposited on the top surface of the low- n RWG structure by dip-coating method, followed by covering with aqueous solution. θ and ϕ_i ($i = 1, 2, 3$) denote the angles of the excitation light and the emission light with respect to the surface normal, respectively. Λ denotes the grating period. The dashed rectangular indicates one unit cell for calculating the electric field intensity distribution in the RWG structure at resonance wavelength.

Figure 1b shows the design of $\text{NaYF}_4:\text{Yb}^{3+}, \text{Tm}^{3+}@ \text{NaYF}_4:\text{Yb}^{3+}, \text{Nd}^{3+}@ \text{NaYF}_4$ CSS UCNPs, where β -phase sodium yttrium fluoride (β - NaYF_4) nanocrystals were chosen as the host material because of their good chemical stability and low phonon cutoff energy (350 cm^{-1}), which can lower the non-radiative relaxation and yield higher UCL

efficiency [8]. Experimentally, β - NaYF_4 -based nanocrystals were co-doped with 20% Yb^{3+} sensitizers and 2% Tm^{3+} activators, acting as the luminescence core (see Figure 1b), with the same procedure as reported in Ref. [42]. In the active shell layer, we then doped two sensitizers, i.e., Nd^{3+} and Yb^{3+} dopants, into the NaYF_4 nanocrystal lattice, aiming to switch the excitation wavelength from 980 to 793 nm. The Nd^{3+} sensitizers were doped at a high ratio (40%) in the active shell layer to harvest excitation photons at 793 nm wavelength. A relatively high doping ratio of Yb^{3+} ions was intentionally incorporated in both the core (20%) and the active shell (10%), acting as the energy migrator, to extract the absorbed energy from the Nd^{3+} sensitizers, then transferring interfacial energy through the Yb^{3+} sub-lattice and finally sensitizing the activator ions (Tm^{3+}) in the core, as illustrated in Figure 1a. The outermost inactive shell was used to reduce the UCL deleterious effect of the Nd^{3+} and Yb^{3+} sensitizers at the surface of the active shell layer to improve the UCL intensity.

2. Materials and Methods

2.1. Chemicals

Yttrium(III) chloride (YCl_3 , anhydrous powder, 99.99%), ytterbium(III) chloride (YbCl_3 , anhydrous powder, 99.9%), thulium(III) chloride (TmCl_3 , anhydrous powder, 99.9%), neodymium (III) chloride (NdCl_3 , anhydrous powder, 99.99%), and ammonium fluoride (NH_4F , anhydrous 99.99%) were purchased from Sigma–Aldrich and kept in a dry box. Sodium oleate (97%) was brought from TCI America. Oleic acid (OA, technical grade, 90%), 1–octadecene (ODE, technical grade, 90%), and tetraethyl orthosilicate (TEOS, 98%) were purchased from Sigma-Aldrich.

2.2. Synthesis of $\text{NaYF}_4:\text{Yb}^{3+},\text{Tm}^{3+}$ Core UCNPs

The monodispersed β -phase $\text{NaYF}_4:\text{Yb}^{3+},\text{Tm}^{3+}$ UCNPs were synthesized using a similar protocol in Ref. [42]. A typical procedure is as follows: 0.78 mmol of YCl_3 , 0.2 mmol of YbCl_3 , 0.02 mmol of TmCl_3 was mixed 6 mL of OA, and 15 mL of ODE in a reaction flask. Under a continuous flow of nitrogen gas, the reaction mixture was heated to 160 °C and continuously stirred to get a transparent yellowish solution. Next, the solution was placed into a vacuum oven and degassed at 110 °C for 1 h. After cooling down to ≈ 60 °C, 10 mL of methanol solution dissolving 4.0 mmol of NH_4F and 2.5 mmol of NaOH was injected dropwise into the flask, followed by stirring for another 30 min. Afterward, the methanol in the reaction mixture was filtered out by evaporation, followed by heating the obtained solution to 110 °C under a vacuum ambient for 1 h. The solution was further heated at 300 °C and reacted for 45 min under nitrogen protection. After taking out the isomantle, the reaction solution was rapidly cooled by blowing a nitrogen stream from the outside and then poured into the centrifuge tubes. The as-synthesized nanoparticles were subsequently precipitated at the bottom of the centrifuge tube by rotating at 6000 r.p.m for 10 min. Finally, these UCNPs were washed with cyclohexane/ethanol (1:1 v/v) two more times, followed by redispersing and storing in cyclohexane for further use.

2.3. Synthesis of $\text{NaYF}_4:\text{Yb}^{3+},\text{Tm}^{3+}@\text{NaYF}_4:\text{Yb}^{3+},\text{Nd}^{3+}$ Core@Shell UCNPs

The optimal content of sensitizers (40% of Nd^{3+} and 10% of Yb^{3+}) co-doped in the active shell layer was reported in ref. [39], which was chosen as the guideline for the synthesis of Nd^{3+} -doped multilayer UCNPs in this study. The shell precursor containing 0.25 mmol of YCl_3 , 0.05 mmol of YbCl_3 , and 0.2 mmol of NdCl_3 was mixed with 6 mL of OA and 15 mL of ODE in a reaction flask, followed by heating to 160 °C under a nitrogen atmosphere to form a clear solution. After cooling down to ≈ 60 °C, the stock solution of the $\text{NaYF}_4:\text{Yb}^{3+},\text{Tm}^{3+}$ core nanoparticles in cyclohexane (20 mL) was added along with the methanol solution (10 mL) containing NH_4F (2.0 mmol) and NaOH (1.25 mmol). The as-obtained solution was stirred for another 40 min and then heated to 110 °C to extract cyclohexane and methanol. Subsequently, the solution was heated to 290 °C and maintained for 1 h under the nitrogen atmosphere, followed by cooling down to room

temperature. The resulting nanoparticles were washed and collected with a similar process as described for the UCNP cores and then stored in cyclohexane.

2.4. Synthesis of $\text{NaYF}_4:\text{Yb}^{3+},\text{Tm}^{3+}@\text{NaYF}_4:\text{Yb}^{3+},\text{Nd}^{3+}@\text{NaYF}_4$ Core@Shell@Shell UCNPs

First, the mixture containing 0.5 mmol of YCl_3 , 6 mL of oleic acid and 15 mL of 1-octadecene was vigorously stirred under nitrogen atmosphere at 160 °C until the solution became transparent. After cooling down naturally to ≈ 60 °C, 10 mL of the $\text{NaYF}_4:\text{Yb}^{3+},\text{Tm}^{3+}@\text{NaYF}_4:\text{Yb}^{3+},\text{Nd}^{3+}$ core-shell nanoparticles in cyclohexane were added into the reaction along with a fresh methanol solution (10 mL) containing NH_4F (2 mmol) and NaOH (1.25 mmol). To extract the low boiling point solvents (cyclohexane and methanol), the reaction was allowed to degas to 110 °C and then stirred for another 40 min. Under the nitrogen ambient, the solution was heated to 290 °C and kept for 1 h, which was followed by cooling down to room temperature. Next, the resulting CSS-structured nanoparticles were washed and collected with a similar process. Finally, the as-prepared CSS UCNPs were stored in cyclohexane for further experiment.

2.5. Fabrication of UCNPs Deposited Low-n RWG Structure

The low-n RWG structure, with 3 μm thick of low-n mesoporous silica film, was initially fabricated using a process sequence involving multiple coating, interference lithography, molding, imprinting and electron-beam deposition, as presented in our previous study [42,48–51]. Afterward, the $\text{NaYF}_4:\text{Yb}^{3+},\text{Tm}^{3+}@\text{NaYF}_4:\text{Yb}^{3+},\text{Nd}^{3+}@\text{NaYF}_4$ CSS UCNPs dispersed into cyclohexane were dip-coated on the top surface of the low-n RWG structure. To evaporate the residual cyclohexane, the dip-coated sample was subsequently baked at 80 °C for 1 h on a hot plate. Finally, an aqueous solution was flooded onto the top of the UCNPs deposited low-n RWG structure, which was followed by encapsulating with a cover glass slide, as shown in Figure 1c.

2.6. UCL and Lifetime Measurement

The optical measurements were performed using a home-built system, similar to that reported in ref. [42]. The excitation light source for both UCL and lifetime measurements was either a 976 nm continuous-wave diode laser (BL976-PAG900, Thorlabs, Newton, NJ, US) or a 793 nm Ti:sapphire laser, depending on which excitation wavelength was chosen. The desired excitation power was adjusted using a variable attenuator, which was intrinsically the combination of a polarizer and a half-wave plate ($\lambda/2$). A red filter glass (RG) was used to block the undesired ambient light in the UV–VIS range, and it allows only the NIR light to excite the UCNP samples. The UCL signal was collected by a pair of lenses and delivered to an Andor Shamrock spectrometer (SR-500i, Oxford Instruments, Oxfordshire, UK) through an optical fiber. Noting also that an IR filter (KG3) was inserted directly in front of the optical fiber to block out the NIR excitation light. To measure the UCL lifetime, we inserted a mechanical chopper to modulate the intensity of the excitation laser light, and then the emitted UCL signal was acquired by a photomultiplier tube (PMT). To precisely assess the lifetime of the 450 nm emission, a 450 nm interference filter was inserted before the PMT.

2.7. Simulations

Rigorous coupled-wave analysis (RCWA) modal was employed to determine resonance wavelength and local electric-field intensity distribution in the RWG structure. For simplicity's sake, we calculated the GMR effect for a unit cell, which was defined as one period of the low-n RWG structure (as illustrated in the dashed rectangle in Figure 1c). The incident light was transverse electric (TE) polarized and propagated along the (xz)-plane from the top surface of the cover glass (see Figure 1c). The harmonics were retained at 25 in the plane wave truncation, in both directions of x - and z -axis, for all the simulations.

2.8. Characterizations

The crystalline structure of nanoparticles was determined by powder X-ray diffraction pattern using a diffractometer (Bruker APEX, Billerica, Massachusetts, USA). The size and morphology of the as-synthesized UCNPs were examined with TEM (JEOL–JEM 2010) and high-resolution TEM (HR–TEM, JEM-2100, JEOL, Tokyo, Japan). Quantitative analysis of elements in UCNPs was examined with energy–dispersive X-ray (EDX) spectroscopy of the FESEM (JSM–6500F, JEOL, Tokyo, Japan). UV–Vis–NIR absorption spectra of UCNPs in the wavelength range of 400–1100 nm were obtained by a UV–VIS–NIR spectrometer (Varian Cary 50, Agilent, Santa Clara, California, USA). The transmission spectra of the UCNPs-deposited low–n RWG were characterized with an Andor Shamrock spectrometer (SR-500i, Oxford Instruments, Oxfordshire, UK).

3. Results and Discussions

3.1. Characterization of UCNPs

Figure 2 presents the morphologies and sizes of as-prepared (a) core (C), (b) core@shell (CS), and (c) core@shell@shell (CSS) UCNPs characterized by TEM. As shown in Figure 2a, the $\text{NaYF}_4:\text{Yb}^{3+},\text{Tm}^{3+}$ core UCNPs are highly uniform and monodispersed with an average diameter of 30 ± 1 nm. Figure 2b,c display the TEM images of $\text{NaYF}_4:\text{Yb}^{3+},\text{Tm}^{3+}@\text{NaYF}_4:\text{Yb}^{3+},\text{Nd}^{3+}$ CS and $\text{NaYF}_4:\text{Yb}^{3+},\text{Tm}^{3+}@\text{NaYF}_4:\text{Yb}^{3+},\text{Nd}^{3+}@\text{NaYF}_4$ CSS UCNPs. The average particle size was increased to 35 ± 1.4 nm when a $\text{NaYF}_4:\text{Yb}^{3+},\text{Nd}^{3+}$ active shell was grown onto the core of $\text{NaYF}_4:\text{Yb}^{3+},\text{Tm}^{3+}$. Since the active shell and core were comprised of similar crystalline structures and compositions, diffraction contrast from Ln^{3+} dopant ions could not directly be observed, as witnessed by the TEM images. With the further inclusion of an inactive NaYF_4 shell, the average diameter of the nanoparticles was up to 40 ± 1.9 nm, indicating the coating of the thin inactive shell with a thickness of 2.5 nm (Figure 2c). Figure 2d displays the HR–TEM image of a single CSS nanoparticle revealing a lattice fringe with the d -spacing of 0.518 nm, which is associated with the (100) lattice planes of the β -phase NaYF_4 .

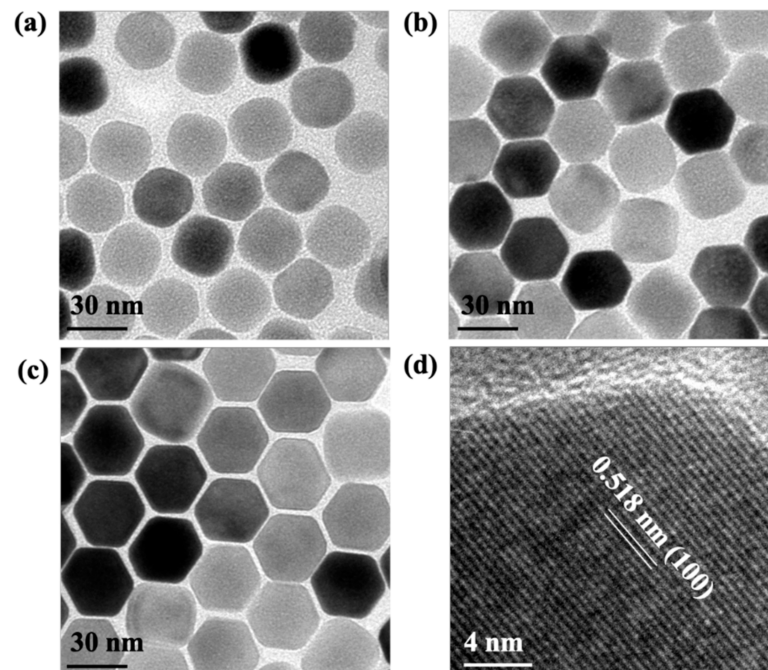


Figure 2. TEM images of: (a) C (b) CS, (c) CSS UCNPs. (d) HRTEM image of a single CSS UCNP.

The high-purity β -phase of the C, CS, and CSS UCNPs were examined using XRD measurement (see Figure S1, in supplementary materials). The XRD analysis clearly indicates that all three types of the UCNPs had identical diffraction peaks to those of the

pure β -phase NaYF_4 , according to the standard data of JCPDS 16–0334. The result reveals that the growth of the active and inactive shell layers did not affect the β -phase structure of NaYF_4 nanocrystals: all characteristic diffraction peaks of β -phase NaYF_4 crystal still remained. The EDX spectroscopy was also used to identify the elemental composition of the $\text{NaYF}_4:\text{Yb}^{3+},\text{Tm}^{3+}$ core and $\text{NaYF}_4:\text{Yb}^{3+},\text{Tm}^{3+}@\text{NaYF}_4:\text{Yb}^{3+},\text{Nd}^{3+}$ CS UCNPs. As shown in Figure S2a,b, the results confirmed the basic elements such as Na, F, Y, Yb, and Tm in both samples. The Nd^{3+} ions only presented in the CS nanoparticles (see Figure S2b), which reveals the successful synthesis of the Nd^{3+} -doped multilayered UCNPs, allowing the generation of UCL emission under the excitation at 793 nm.

3.2. Nanoparticles Engineering for Enhancing UCL Intensity

To further confirm the presence of the sensitizing ions (Yb^{3+} and Nd^{3+}) in the as-prepared UCNPs, the absorption spectra of the C and CS UCNPs were taken. As presented in Figure 3a, the absorption band at 976 nm in both spectra is assigned to the ${}^2\text{F}_{7/2} \rightarrow {}^2\text{F}_{5/2}$ transition of Yb^{3+} ions. The multiple absorption bands at 863, 793, 742, 575, and 521 (nm) in the absorption spectra of the CS UCNPs pertaining to the transitions of Nd^{3+} ions from ${}^4\text{I}_{9/2}$ to ${}^4\text{F}_{3/2}$, ${}^4\text{F}_{5/2}$, ${}^4\text{F}_{7/2}$, ${}^4\text{G}_{5/2}$, and ${}^4\text{G}_{7/2}$, respectively, thereby indicating the formation of the Nd^{3+} -sensitized active shell layer surrounding the $\text{NaYF}_4:\text{Yb}^{3+},\text{Tm}^{3+}$ core. Moreover, these spectra clearly shows that the absorption coefficient at 793 nm of Nd^{3+} is much larger than that at 976 nm of Yb^{3+} , allowing a dramatic increase in the photon-harvesting efficiency of the Nd^{3+} -sensitized upconversion process.

We next turn to the examination of UCL spectra of the three kinds of UCNPs (C, CS, CSS) under both excitation wavelengths of 976 and 793 nm with 20 W/cm^2 intensity. Excited with a 976 nm CW laser light emitted from a diode laser, the CSS UCNPs produced the highest UCL intensity, which was two to four times higher than those emitted from the CS and C UCNPs (see Figure 3b and its inset). After growing the active and inactive shells, the UCL peak positions did not have any obvious shift, supporting the assumption that the energy levels of Tm^{3+} ions remained unchanged. Figure 3c displays the UCL spectra of the C, CS, and CSS UCNPs excited with the CW Ti:sapphire laser at the wavelength of 793 nm. Since the $\text{NaYF}_4:\text{Yb}^{3+},\text{Tm}^{3+}$ core UCNPs have no absorption at 793 nm as seen in Figure 3a, UCL emission was not observed from this sample. As clearly displayed in Figure 3c and its inset, the intensities of all the UCL emission bands of the CSS UCNPs were enhanced by four to eight times, compared to those emitted from the CS counterparts. It implies that the NaYF_4 inactive outer shell can protect the $\text{NaYF}_4:\text{Yb}^{3+},\text{Nd}^{3+}$ active shell, reaching its goal of inhibiting the UCL quenching induced by the organic impurities, ligands, and solvents on the surface of the active shell. Figure 3d and its inset show a comparison of the UCL emission intensities of the CSS UCNPs obtained under the excitations at 793 nm and 976 nm with the same excitation intensity. It is clear that UCL intensities excited with a 793 nm laser beam are about six to nine times higher than those excited with a 976 nm laser beam, which is an enhancement ascribed to the larger absorption cross-section of Nd^{3+} at 793 nm. The inset shows a photograph of the UCL emissions from the CSS UCNPs sample under the excitation of two parallel narrow laser beams at NIR wavelengths of 793 and 976 nm of equal incident power. Here, we clearly demonstrated that by structural engineering of the UCNPs, the UCL intensities are improved by a factor of up to nine.

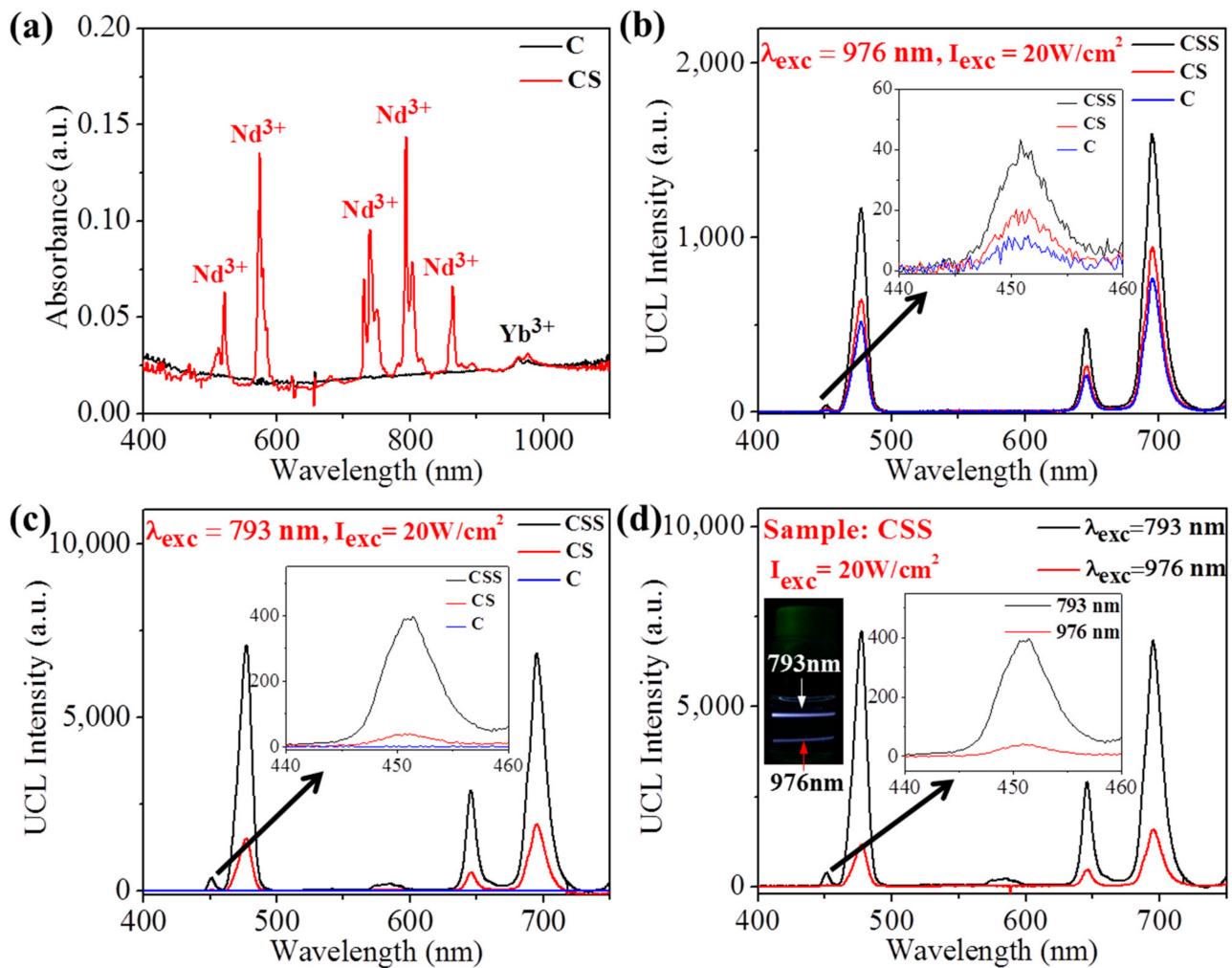


Figure 3. (a) UV–VIS–NIR absorption spectra of C and CS UCNP samples dispersed into cyclohexane at a concentration of 0.1 mmol/mL. UCL spectra of as-synthesized samples (C, CS, CSS) in the wavelength range of 400–750 nm under (b) 976 nm excitation and (c) 793 nm excitation. Insets show UCL emission spectra of these samples in the wavelength range of 440–460 nm. (d) UCL emission spectra of the CSS sample under the excitation at 793 and 976 nm, inset shows its enlarged view in the wavelength range of 440–460 nm and a photograph of the CSS sample under the excitation of two parallel narrow beams at 793 and 976 nm.

3.3. Photonic Engineering for Enhancing UCL Intensity

In order to further improve the UCL intensity of the as-prepared UCNP samples, we deposited the CSS UCNP samples ($\text{NaYF}_4:\text{Yb}^{3+},\text{Tm}^{3+}@\text{NaYF}_4:\text{Yb}^{3+},\text{Nd}^{3+}@\text{NaYF}_4$) atop a low- n RWG structure (see Figure 1c). The RCWA simulation was used to search the optimal structure and the corresponding excitation resonance conditions for enhancing UCL intensity through calculating the electric field intensity ($|E|^2$) distribution atop the low- n RWG structure. The simulated RWG structure is composed of a cover glass slide, an aqueous solution layer, a TiO_2 waveguide layer, a low- n mesoporous silica grating layer treated as an effective medium, and a glass substrate, as shown in Figure 1c. The overall structure parameters of the low- n RWG in this design are as follows: the TiO_2 thickness (T_{TiO_2}) = 60 nm, the low- n mesoporous silica thickness ($T_{\text{mp-silica}}$) = 3 μm , the modulation depth (D_m) = 100 nm, and the grating period (Λ) = 550 nm. The refractive indices at the VIS–near IR wavelength range of materials in the low- n RWG sample are as follows: cover glass slide $n_{\text{cover glass}} = 1.5$, aqueous solution $n_{\text{aq}} = 1.33$, TiO_2 $n_{\text{TiO}_2} = 2.06$, mesoporous silica $n_{\text{mp-silica}} = 1.22$ [42], and glass $n_{\text{glass}} = 1.5$. Figure 4a presents the measured and simulated TE transmission spectra of the low- n RWG sample. To attain the GMR for the excitation wavelength of UCNP samples

at 793 nm, the incident angle was tuned to $\theta = 1.5^\circ$. Both experimental (black curve) and simulation (red curve) results indicate that a transmission dip, i.e., a GMR, appears at 793 nm (the experiment is not as contrasted as the prediction, which is probably because of effects such as finite beam size, etc.). Under this condition, i.e., $\lambda = 793$ nm and $\theta = 1.5^\circ$, which we refer to as a resonant excitation condition, a strong local field can be produced upon the TiO_2 surface as a consequence of the evanescent field of the guided mode that concentrates a large fraction of the incident beam power in the GMR effect (see Figure 4b). This large field indicates that the low- n RWG structure is suitable for enhancing the UCL of Nd^{3+} -sensitized CSS UCNP in an aqueous solution. Therefore, we deposited the CSS UCNP on the low- n RWG sample and illuminated the sample with a collimated Ti:sapphire laser beam at 793 nm wavelength with 5 W/cm^2 intensity under resonant and non-resonant excitation conditions. Figure 4c depicts the UCL spectra of the low- n RWG deposited with CSS UCNP obtained at $\theta = 1.5^\circ$ (on-resonance), $\theta = 2.0^\circ$ (off-resonance), and non-RWG (planar) area of the sample. It clearly shows that the UCL intensities from all emission peaks were dramatically increased as the sample was illuminated under resonant condition, i.e., $\theta = 1.5^\circ$ compared to those obtained at other angles, for example at $\theta = 2.0^\circ$, and non-RWG area thanks to the strong interaction between the local field built up atop of the low- n RWG and UCNP.

In addition to the excitation resonance effect, the extraction resonance effect was employed to further enhance the UCL intensity of CSS UCNP on the low- n RWG structure by collecting the emission of UCNP at the GMR condition corresponding to the peak wavelengths of the UCL of the CSS UCNP deposited on the low- n RWG sample. This was achieved by illuminating the sample at the resonant excitation condition and scanning the detection angle (φ) from 17° to 62° for optimal UCL intensities. Figure 4d displays the UCL intensities of the characteristic emission peaks (450, 480, 645 nm) as a function of the collection angle (φ -angles). It is clear that the UCL emission of these peaks were promoted two to four times at $\varphi = 22^\circ$, 46° , and 53° , which satisfied the GMR (i.e., emission resonance) conditions for 645, 480, and 450 nm emission wavelengths, respectively. These enhancements occurred when the GMR peaks of the low- n RWG deposited with CSS UCNP (see Figure S3a–c) coincide with the corresponding emission wavelengths of UCNP. In such conditions, the upconversion light, of spontaneous nature in terms of coherence, is largely extracted, since the large fraction of emitted photons initially coupled in the guided mode are scattered out at the specific extraction angles given above. Figure S4 presents the UCL decay curve at the 450 nm emission peak, which is measured at the non-RWG area and the RWG area under excitation resonance + extraction resonance. It is clear that the lifetime of the non-RWG sample is longer ($567 \mu\text{s}$) than that of the RWG sample under excitation resonance + extraction resonance ($449 \mu\text{s}$), suggesting that the RWG sample under excitation resonance + extraction resonance can increase the radiative decay rate of the 450 nm emission, thanks to various factors, including the Purcell effect.

To compare the UCL enhancement factors obtained from the photonic engineering approach with two different incident wavelengths 793 and 976 nm, we measured the UCL spectra of the CSS UCNP deposited low- n RWG sample under excitation resonances at 793 and 976 nm with the same excitation intensity, i.e., 5 W/cm^2 . First, the sample was tuned to the resonant angle for each case, i.e., $\theta = 1.5^\circ$ for 793 nm and $\theta = 21^\circ$ for 976 nm (see Figures 4a and S3d). As displayed in Figure 5a, the UCL emissions of the characteristic peaks (450, 480, and 650 nm) obtained with the 793 nm excitation were three to six times higher than those obtained with the 976 nm excitation. We found that the local electric field enhancement factors relative to the field atop of the TiO_2 surface for both excitation resonance conditions are quite close (Figures 4b and S5), so that the higher UCL intensities obtained with the 793 nm excitation configuration were attributed to the larger absorption cross-section of Nd^{3+} at 793 nm. The use of 793 nm laser excitation not only can greatly improve the UCL efficiency of UCNP but also can overcome the problems associated with overheating and low penetration, which are frequently faced and incur penalties in many biological applications.

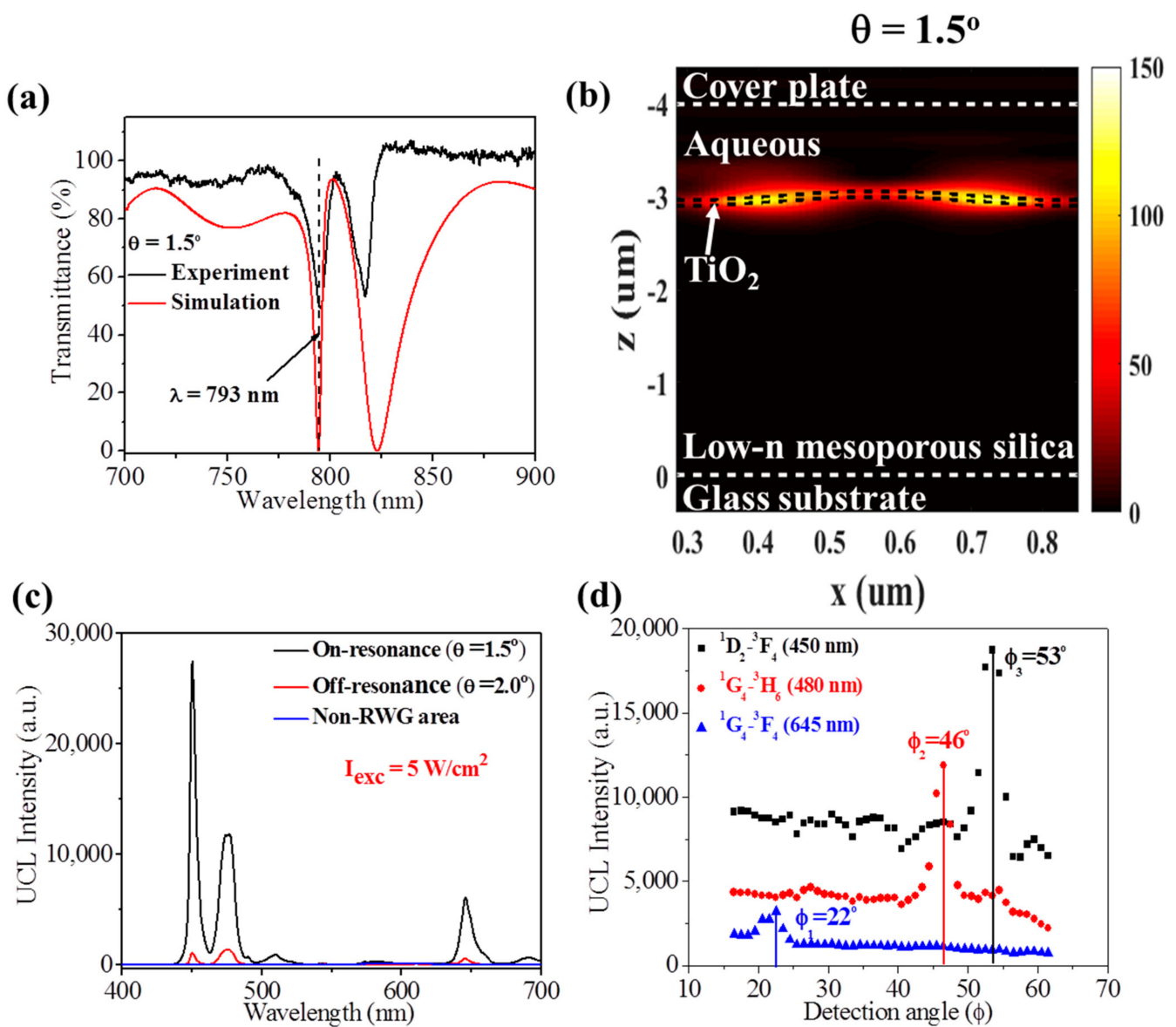


Figure 4. (a) Measured and simulated transmission spectra of the low-n RWG structure at the incident angle of 1.5° . (b) Simulated TE mode electric-field intensities ($|E|^2$) under resonant excitation condition ($\lambda = 793$ nm, $\theta = 1.5^\circ$) of the low-n RWG flooded with aqueous solution. (c) UCL spectra measured at the RWG area of the low-n RWG deposited with CSS UCNP under on-resonance ($\theta = 1.5^\circ$) and off-resonance ($\theta = 2.0^\circ$) and that measured at the non-RWG area of the sample. (d) UCL emission intensities at the characteristic emission peaks of the CSS UCNP deposited on the top surface of the low-n RWG sample versus the detection angle (ϕ) under resonant excitation condition ($\theta = 1.5^\circ$).

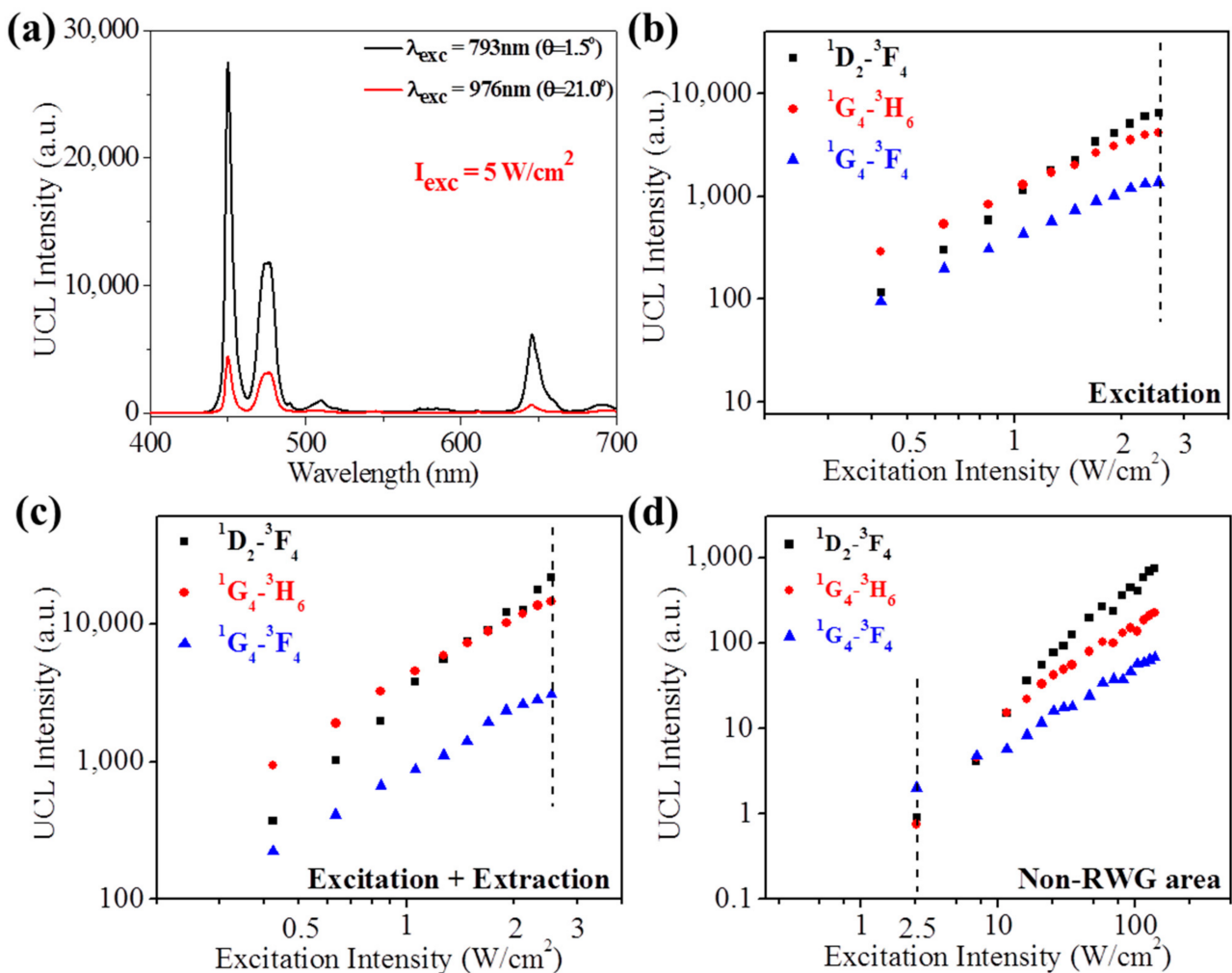


Figure 5. (a) UCL spectra of the CSS UCNP deposited on the top surface of the low- n RWG structures under excitation resonances with two different incident wavelengths at $\lambda = 793$ nm ($\theta = 1.5^\circ$) and $\lambda = 976$ nm ($\theta = 21.0^\circ$). Excitation intensity dependences of three main UCL peak intensities obtained from the CSS UCNP deposited on the low- n RWG sample under (b) excitation resonance, (c) excitation resonance + extraction resonance, and (d) the UCL obtained from a non-RWG area.

Figure 5b–d show the logarithmic plot of three UCL intensities versus the excitation intensity in the range of 0.4–2.5 W/cm^2 under conditions of excitation resonance, excitation resonance + extraction resonance, and non-RWG area, respectively. As revealed in Figure 5b–d, UCL intensities of all emission peaks generated under all three cases increased with the excitation intensity. To quantitatively assess the UCL enhancement factors under the GMR conditions, we compared the UCL intensities obtained at 2.5 W/cm^2 (vertical dash lines marked in Figure 5b–d) for both RWG and non-RWG samples. From Figure 5b,d, the enhancement factors for emission wavelengths (λ_e) at 450, 480, and 645 nm under excitation resonance were determined to be 7.2×10^3 , 5.5×10^3 , and 6.9×10^2 , respectively. Furthermore, these enhancement factors were further increased by 3.4, 3.5, and 2.4 folds, respectively, after adding the extraction resonance to the excitation resonance, as indicated in Figure 5b,c.

3.4. Overall Enhancement Factor of All the Strategies Combined

Table 1 summarizes the overall UCL enhancement factors of three main UCL peaks offered by all strategies adopted in this study, i.e., surface passivation, Nd^{3+} doping for the nanoparticle engineering and excitation resonance + extraction resonance provided by the low- n RWG structure for the photonic engineering. Let us remind the origins of each of the three factors: the UCL enhancement factors through surface passivation

were determined by comparing the UCL intensities of two samples, i.e., the C and CSS UCNP, under 976 nm excitation, as displayed in Figure 3b. With the coating of the active and inactive shells, the UCL emissions of the characteristic peaks at 450, 480, and 645 nm were enhanced 4.9, 2.7, and 2.8 times, respectively. To get the UCL enhancement factors offered by the Nd^{3+} doping strategy, the UCL intensities of CSS UCNP under excitations at 793 and 976 nm were compared, as presented in Figure 3d. The enhancement factors at these three aforementioned emission wavelengths were found to be 9.2, 6.1, and 6.1, respectively. Together with the emission enhancement factors obtained from the excitation resonance + extraction resonance provided by the low- n RWG structure, the total enhancement factor of the UCL emission at 450 nm was up to 1.1×10^6 fold. The huge enhancement of UCL intensity provided by the combination of the presented approaches is extremely useful for the applications of UCNP in the biosensing and bioimaging field. It can greatly assist in considering UCNP markers for these applications on a similar footing with downconversion classical ones, balancing the remaining discrepancy in luminescence level with the known drawbacks of downconversion (bleaching, heating, etc.) that are absent in UCNP.

Table 1. Comparison of enhancement factors obtained at the emission wavelengths (λ_e) 450, 480, and 645 nm of the Tm^{3+} -doped UCNP using the different strategies reported in this work.

λ_e (nm)	Enhancement Factor		
	450	480	645
Surface passivation	4.9	2.7	2.8
Nd^{3+} doping	9.2	6.1	6.1
Excitation resonance	7.2×10^3	5.5×10^3	6.9×10^2
Extraction resonance	3.4	3.5	2.4
Total	1.1×10^6	3.2×10^5	2.8×10^4

4. Conclusions

Through the synergy approach presented in this work, we showed that the UCL intensity of Tm^{3+} -doped UCNP was remarkably enhanced more than 10^6 -fold, which is particularly valuable for practical applications in bioimaging and biosensing. First, Tm^{3+} -doped core UCNP were coated with two engineered shells for two different purposes. The inclusion of the active middle shell serves to additionally dope Nd^{3+} sensitizers capable of blue-shifting the excitation wavelength from 976 to 793 nm, which has been deemed as a suitable excitation wavelength with negligible risk for bio-tissues. The outer inactive shell was further grown to reduce the surface quenching associated with Nd^{3+} and Yb^{3+} sensitizers by shielding them from the aqueous environment. The UCL intensity of the Nd^{3+} -doped CSS UCNP is more than one order of magnitude higher than that of the conventional Yb^{3+} -doped core UCNP, showing the role of surface passivation and Nd^{3+} sensitizing for enhancing UCL emission intensity. To achieve the desired UCL intensity for biological application on demand, we deposited these CSS UCNP on top of the low- n RWG structure. Thanks to the excitation resonance offered by the low- n RWG, a strong local field could be built upon its top surface, which dramatically enhanced UCL intensity about 10^4 times. In addition, the UCL intensity of the UCNP was further increased two to three times under excitation resonance + extraction resonance (reminiscent of earlier attempts in DNA biochips [52]). Combining all these effects together, the UCL intensity of CCS UCNP was enhanced more than 10^6 times compared to Yb^{3+} -doped core UCNP on planar substrates. We believe that the extraordinary enhanced UCL emission generated by the 793 nm excitation light source opens up great prospects for the applications of UCNP in the bioimaging and biosensing field.

Supplementary Materials: The following are available online at <https://www.mdpi.com/article/10.3390/cryst11101187/s1>, The physical properties of the as-prepared UCNPs (XRD pattern and EDX spectra); the angle-resolved transmission spectra of the CSS UCNPs deposited low-n RWG sample in the specific detection and excitation angles; the UCL lifetime of the emission at 450 nm of the UCNPs doped low-n RWG sample at the different conditions: Excitation + Extraction resonance, Non-RWG area; calculated TE mode electric-field intensities ($|E|^2$) under resonant excitation condition ($\lambda = 976$ nm, $\theta = 21^\circ$) of the low-n RWG are provided in the Supplementary Materials.

Author Contributions: C.-C.H. planned the project and supervised the overall project. D.T.V. performed the simulation, designed the experiments and the synthesis of UCNPs. Y.-C.T. fabricated the low-n RWG and performed UCL measurement. Q.M.L. instructed the synthesis of UCNPs. S.-W.K. instructed the fabrication of low-n thin film. J.-Y.L., N.D.L. consulted the UCL measurement of the low-n RWG sample. H.-C.K. and H.B. instructed to perform the simulation. The manuscript was written through the contributions of all authors. All authors have read and agreed to the published version of the manuscript.

Funding: This work was supported by the Ministry of Science and Technology, Taiwan, under grant Nos. MOST 107-2112-M-194-001-MY3, MOST 107-2923-M-194-001-MY3 and Agence Nationale de la Recherche (ANR-17-CE09-0047).

Conflicts of Interest: The authors declare no conflict of interest.

References

1. Wang, F.; Liu, X. Recent advances in the chemistry of lanthanide-doped upconversion nanocrystals. *Chem. Soc. Rev.* **2009**, *38*, 976–989. [[CrossRef](#)]
2. Zhang, F. *Photon Upconversion Nanomaterials*; Springer: Berlin/Heidelberg, Germany, 2015.
3. Wu, S.; Butt, H.J. Near-infrared-sensitive materials based on upconverting nanoparticles. *Adv. Mater.* **2016**, *28*, 1208–1226. [[CrossRef](#)]
4. Auzel, F. Upconversion and anti-Stokes processes with f and d ions in solids. *Chem. Rev.* **2004**, *104*, 139–174. [[CrossRef](#)]
5. Auzel, F. History of upconversion discovery and its evolution. *J. Lumin.* **2020**, *223*, 116900. [[CrossRef](#)]
6. Anderson, R.B.; Smith, S.J.; May, P.S.; Berry, M.T. Revisiting the NIR-to visible upconversion mechanism in β -NaYF₄:Yb³⁺,Er³⁺. *J. Phys. Chem. Lett.* **2014**, *5*, 36–42. [[CrossRef](#)] [[PubMed](#)]
7. Haase, M.; Schafer, H. Upconverting nanoparticles. *Angew. Chem. Int. Ed.* **2011**, *50*, 5808–5829. [[CrossRef](#)] [[PubMed](#)]
8. Chen, G.; Qiu, H.; Prasa, P.N.; Chen, X. Upconversion nanoparticles: Design, nanochemistry, and applications in theranostics. *Chem. Rev.* **2014**, *114*, 5161–5214. [[CrossRef](#)] [[PubMed](#)]
9. Zhou, J.; Liu, Q.; Feng, W.; Sun, Y.; Li, F. Upconversion luminescent materials: Advances and applications. *Chem. Rev.* **2015**, *115*, 395–465. [[CrossRef](#)] [[PubMed](#)]
10. Chen, C.; Li, C.; Shi, Z. Current advances in lanthanide-doped upconversion nanostructures for detection and bioapplication. *Adv. Sci.* **2016**, *3*, 1600029. [[CrossRef](#)]
11. Lin, M.; Zhao, Y.; Wang, S.Q.; Liu, M.; Duan, Z.H.; Chen, Y.M.; Li, F.; Xu, F.; Lu, T.J. Recent advances in synthesis and surface modification of lanthanide-doped upconversion nanoparticles for biomedical applications. *Biotechnol. Adv.* **2012**, *30*, 1551–1561. [[CrossRef](#)]
12. Zheng, W.; Huang, P.; Tu, D.; Ma, E.; Zhu, H.; Chen, X. Lanthanide-doped upconversion nano-bioprobes: Electronic structures, optical properties, and biodetection. *Chem. Soc. Rev.* **2015**, *44*, 1379–1415. [[CrossRef](#)]
13. Zhou, J.; Liu, Z.; Li, F. Upconversion nanophosphors for small-animal imaging. *Chem. Soc. Rev.* **2012**, *41*, 1323–1349. [[CrossRef](#)]
14. Zhou, B.; Shi, B.; Jin, D.; Liu, X. Controlling upconversion nanocrystals for emerging applications. *Nat. Nanotechnol.* **2015**, *10*, 924–936. [[CrossRef](#)]
15. Vu, D.T.; Le, T.T.V.; Hsu, C.C.; Lai, N.D.; Hecquet, C.; Benisty, H. Positive role of upconversion nanophosphors on resonant surfaces for ultra-compact filter-free bio-assays. *BioMed Opt. Express* **2021**, *12*, 1–19. [[CrossRef](#)]
16. Vu, D.T.; Vu Le, T.T.; Nguyen, V.N.; Le, Q.M.; Wang, C.R.C.; Chau, L.K.; Yang, T.S.; Chan, M.W.Y.; Lee, C.I.; Ting, C.C.; et al. Gold nanorods conjugated upconversion nanoparticles nanocomposites for simultaneous bioimaging, local temperature sensing and photothermal therapy of OML-1 oral cancer cells. *Int. J. Smart Nano Mater.* **2021**, *12*, 49–71. [[CrossRef](#)]
17. Sedlmeier, A.; Gorris, H.H. Surface modification and characterization of photon-upconverting nanoparticles for bioanalytical applications. *Chem. Soc. Rev.* **2015**, *44*, 1526–1560. [[CrossRef](#)]
18. Liu, Q.; Zhang, Y.; Peng, C.S.; Yang, T.; Joubert, L.M.; Chu, S. Single upconversion nanoparticle imaging at sub-10 W cm⁻² irradiance. *Nat. Photonics* **2018**, *12*, 548–553. [[CrossRef](#)] [[PubMed](#)]
19. Wang, Y.F.; Liu, G.Y.; Sun, L.D.; Xiao, J.W.; Zhou, J.C.; Yan, C.H. Nd³⁺-Sensitized upconversion nanophosphors: Efficient in vivo bioimaging probes with minimized heating effect. *ACS Nano* **2013**, *7*, 7200–7206. [[CrossRef](#)] [[PubMed](#)]

20. Wang, D.; Chen, C.; Ke, X.; Kang, N.; Shen, Y.; Liu, Y.; Zhou, X.; Wang, H.; Chen, C.; Ren, L. Bioinspired near-infrared-excited sensing platform for in vitro antioxidant capacity assay based on upconversion nanoparticles and a dopamine–melanin hybrid system. *ACS Appl. Mater. Interfaces* **2015**, *7*, 3030–3040. [[CrossRef](#)]
21. Wang, N.; Yu, X.; Zhang, K.; Mirkin, C.A.; Li, J. Upconversion nanoprobe for the ratiometric luminescent sensing of nitric oxide. *J. Am. Chem. Soc.* **2017**, *139*, 12354–12357. [[CrossRef](#)] [[PubMed](#)]
22. Qiao, R.; Liu, C.; Liu, M.; Hu, H.; Liu, C.; Hou, Y.; Wu, K.; Lin, Y.; Liang, J.; Gao, M. Ultrasensitive in vivo detection of primary gastric tumor and lymphatic metastasis using upconversion nanoparticles. *ACS Nano* **2015**, *9*, 2120–2129. [[CrossRef](#)]
23. Lai, J.; Shah, B.P.; Zhang, Y.; Yang, L.; Lee, K.B. Real-time monitoring of ATP-responsive drug release using mesoporous-silica-coated multicolor upconversion nanoparticles. *ACS Nano* **2015**, *9*, 5234–5245. [[CrossRef](#)]
24. Wang, C.; Cheng, L.; Liu, Z. Upconversion nanoparticles for photodynamic therapy and other cancer therapeutics. *Theranostics* **2013**, *3*, 317–330. [[CrossRef](#)]
25. Boyer, J.C.; van Veggel, F.C.J.M. Absolute quantum yield measurements of colloidal NaYF₄: Er³⁺, Yb³⁺ upconverting nanoparticles. *Nanoscale* **2010**, *2*, 1417–1419. [[CrossRef](#)]
26. Liu, Q.; Sun, Y.; Yang, T.; Feng, W.; Li, C.; Li, F. Sub-10 nm hexagonal lanthanide-doped NaLuF₄ upconversion nanocrystals for sensitive bioimaging in vivo. *J. Am. Chem. Soc.* **2011**, *133*, 17122–17125. [[CrossRef](#)] [[PubMed](#)]
27. Han, S.; Deng, R.; Xie, X.; Liu, X. Enhancing luminescence in lanthanide-doped upconversion nanoparticles. *Angew. Chem. Int. Ed.* **2014**, *53*, 11702–11715. [[CrossRef](#)] [[PubMed](#)]
28. Das, A.; Bae, K.; Park, W. Enhancement of upconversion luminescence using photonic nanostructures. *Nanophotonics* **2020**, *9*, 1359–1371. [[CrossRef](#)]
29. Wilhelm, S. Perspectives for upconverting nanoparticles. *ACS Nano* **2017**, *11*, 10644–10653. [[CrossRef](#)]
30. Lu, Q.; Guo, F.Y.; Sun, L.; Li, A.H.; Zhao, L.C. Silica-/titania-coated, nanoparticles with improvement in upconversion luminescence induced by different thickness shells. *J. Appl. Phys.* **2008**, *103*, 123533. [[CrossRef](#)]
31. Vetrone, F.; Naccache, R.; Mahalingam, V.; Morgan, C.C.; Capobianco, J.A. The active core/active-shell approach: A strategy to enhance the upconversion luminescence in lanthanide doped nanoparticles. *Adv. Funct. Mater.* **2009**, *19*, 2924–2929. [[CrossRef](#)]
32. Chen, X.; Peng, D.; Ju, Q.; Wang, F. Photon upconversion in core–shell nanoparticles. *Chem. Soc. Rev.* **2015**, *44*, 1318–1330. [[CrossRef](#)]
33. Xie, X.; Gao, N.; Deng, R.; Sun, Q.; Xu, Q.H.; Liu, X. Mechanistic investigation of photon upconversion in Nd³⁺-sensitized core–shell nanoparticles. *J. Am. Chem. Soc.* **2013**, *135*, 12608–12611. [[CrossRef](#)] [[PubMed](#)]
34. Wang, D.; Xue, B.; Kong, X.; Tu, L.; Liu, X.; Zhang, Y.; Chang, Y.; Luo, Y.; Zhao, H.; Zhang, H. 808 nm driven Nd³⁺-sensitized upconversion nanostructures for photodynamic therapy and simultaneous fluorescence imaging. *Nanoscale* **2015**, *7*, 190–197. [[CrossRef](#)] [[PubMed](#)]
35. Wiesholler, L.M.; Frenzel, F.; Grauel, B.; Wurth, C.; Resch-Genger, U.; Hirsch, T. Yb, Nd, Er-doped upconversion nanoparticles: 980 nm versus 808 nm excitation. *Nanoscale* **2019**, *11*, 13440–13449. [[CrossRef](#)] [[PubMed](#)]
36. Hao, S.; Chen, G.; Yang, C.; Yang, C.; Shao, W.; Wei, W.; Liu, Y.; Prasad, P.N. Nd³⁺-sensitized multicolor upconversion luminescence from a sandwiched core/shell/shell nanostructure. *Nanoscale* **2017**, *9*, 10633–10638. [[CrossRef](#)] [[PubMed](#)]
37. Chan, M.H.; Liu, R.S. Advanced sensing, imaging, and therapy nanoplatfroms based on Nd³⁺-doped nanoparticle composites exhibiting upconversion induced by 808 nm near-infrared light. *Nanoscale* **2017**, *9*, 18153–18168. [[CrossRef](#)] [[PubMed](#)]
38. Zhong, Y.; Tian, G.; Gu, Y.; Yang, Y.; Gu, L.; Zhao, Y.; Ma, Y.; Yao, J. Elimination of photon quenching by a transition layer to fabricate a quenching-shield sandwich structure for 800 nm excited upconversion luminescence of Nd³⁺-sensitized nanoparticles. *Adv. Mater.* **2014**, *26*, 2831–2837. [[CrossRef](#)]
39. Lu, F.; Yang, L.; Ding, Y.; Zhu, J.J. Highly emissive Nd³⁺-sensitized multilayered upconversion nanoparticles for efficient 795 nm operated photodynamic therapy. *Adv. Funct. Mater.* **2016**, *26*, 4778–4785. [[CrossRef](#)]
40. Purcell, E.M.; Torrey, H.C.; Pound, R.V. Resonance absorption by nuclear magnetic moments in a solid. *Phys. Rev.* **1946**, *69*, 37–38. [[CrossRef](#)]
41. Lin, J.H.; Liou, H.Y.; Wang, C.D.; Tseng, C.Y.; Lee, C.T.; Ting, C.C.; Kan, H.C.; Hsu, C.C. Giant enhancement of upconversion fluorescence of NaYF₄:Yb³⁺, Tm³⁺ nanocrystals with resonant waveguide grating substrate. *ACS Photonics* **2015**, *2*, 530–536. [[CrossRef](#)]
42. Vu, D.T.; Chiu, H.W.; Nababan, R.; Le, Q.M.; Kuo, S.W.; Chau, L.K.; Ting, C.C.; Kan, H.C.; Hsu, C.C. Enhancing upconversion luminescence emission of rare earth nanophosphors in aqueous solution with thousands fold enhancement factor by low refractive index resonant waveguide grating. *ACS Photonics* **2018**, *5*, 3263–3271. [[CrossRef](#)]
43. Wang, H.; Yin, Z.; Wen, X.; Zhou, D.; Cui, S.; Chen, X.; Cui, H.; Song, H. Remarkable enhancement of upconversion luminescence on 2-D anodic aluminum oxide photonic crystals. *Nanoscale* **2016**, *8*, 10004–10009. [[CrossRef](#)]
44. Yin, Z.; Zhu, Y.; Xu, W.; Wang, J.; Xu, S.; Dong, B.; Xu, L.; Zhang, S.; Song, H. Remarkable enhancement of upconversion fluorescence and confocal imaging of PMMA opal/NaYF₄:Yb³⁺, Tm³⁺/Er³⁺ nanocrystals. *ChemComm.* **2013**, *49*, 3781–3783. [[CrossRef](#)]
45. Mao, C.; Min, K.; Bae, K.; Cho, S.; Xu, T.; Jeon, H.; Park, W. Enhanced upconversion luminescence by two-dimensional photonic crystal structure. *ACS Photonics* **2019**, *6*, 1882–1888. [[CrossRef](#)]

46. Wurth, C.; Manley, P.; Voigt, R.; Ahiboz, D.; Becker, C.; Resch-Genger, U. Metasurface enhanced sensitized photon upconversion: Toward highly efficient low power upconversion applications and nanoscale E-field sensors. *Nano Lett.* **2020**, *9*, 6682–6689. [[CrossRef](#)]
47. Gong, C.; Liu, W.; He, N.; Dong, H.; Jin, Y.; He, S. Upconversion enhancement by a dual-resonance all-dielectric metasurface. *Nanoscale* **2019**, *11*, 1856–1862. [[CrossRef](#)]
48. Liu, C.C.; Li, J.G.; Kuo, S.W. Co-template method provides hierarchical mesoporous silicas with exceptionally ultra-low refractive indices. *RSC Adv.* **2014**, *4*, 20262–20272. [[CrossRef](#)]
49. Lin, J.H.; Tseng, C.Y.; Lee, C.T.; Kan, H.C.; Hsu, C.C. Guided-mode resonance enhanced excitation and extraction of two-photon photoluminescence in a resonant waveguide grating. *Opt. Express* **2013**, *21*, 24318–24325. [[CrossRef](#)] [[PubMed](#)]
50. Lin, J.H.; Tseng, C.Y.; Lee, C.T.; Young, J.F.; Kan, H.C.; Hsu, C.C. Strong guided mode resonant local field enhanced visible harmonic generation in an azopolymer resonant waveguide grating. *Opt. Express* **2014**, *22*, 2790–2797. [[CrossRef](#)] [[PubMed](#)]
51. Lai, N.D.; Liang, W.P.; Lin, J.H.; Hsu, C.C.; Lin, C.H. Fabrication of two- and three-dimensional periodic structures by multi-exposure of two-beam interference technique. *Opt. Express* **2005**, *13*, 9605–9611. [[CrossRef](#)] [[PubMed](#)]
52. Choumane, H.; Ha, N.; Nelep, C.; Chardon, A.; Reymond, G.O.; Goutel, C.; Cerovic, G.; Vallet, F.; Weisbuch, C.; Benisty, H. Double interference fluorescence enhancement from reflective slides: Application to bicolor microarrays. *Appl. Phys. Lett.* **2005**, *87*, 031102. [[CrossRef](#)]